Monthly Notices of the ROYAL ASTRONOMICAL SOCIETY

MNRAS **530,** 3043–3050 (2024)
Advance Access publication 2024 April 8

https://doi.org/10.1093/mnras/stae960

A search for intermediate-mass black holes in compact stellar systems through optical emissions from tidal disruption events

Richard T. Pomeroy [1,2] and Mark A. Norris [1]★

[1] *Jeremiah Horrocks Institute, University of Central Lancashire, Preston PR1 2HE, UK*
[2] *Department of Physics and Astronomy, The University of Texas Rio Grande Valley, Brownsville, TX 78520, USA*

Accepted 2024 April 4. Received 2024 April 3; in original form 2023 November 28

ABSTRACT

Intermediate-mass black holes (IMBHs) are expected to exist in globular clusters (GCs) and compact stellar systems (CSSs) in general, but none have been conclusively detected. Tidal disruption events (TDEs), where a star is tidally disrupted by the gravitational field of a black hole, have been observed to occur around the supermassive black holes (SMBHs) found at the centres of galaxies, and should also arise around IMBHs, especially in the dense stellar cores of CSSs. However, to date none have been observed in such environments. Using data from the Zwicky Transient Facility, we search for TDEs associated with CSSs, but none are found. This non-detection allows us to set an upper limit on the TDE rate in CSSs of $n_{\rm TDE,Total} \lessapprox 10^{-7}\,{\rm CSS}^{-1}\,{\rm yr}^{-1}$, which is 2 dex below the observed TDE rate involving SMBHs interacting with 1 $M_\odot$ main-sequence stars in the nuclei of massive galaxies. We also consider ultracompact dwarfs (UCDs) formed through a tidal stripping process in the surveyed volume. On the assumption that these CSSs contain SMBHs and TDE rates are comparable to current observed optical rates in galactic nuclei ($\approx 3.2 \times 10^{-5}\,{\rm gal}^{-1}\,{\rm yr}^{-1}$), we determine an upper limit for the number of UCDs formed through a tidal stripping process in the surveyed volume to be $N_{\rm GC,Strip} < 1.4 \times 10^4$, which we estimate represents < 6 per cent of the population of GCs $>10^6\,M_\odot$.

Key words: stars: black holes – globular clusters: general – transients: tidal disruption events.

1 INTRODUCTION

Tidal disruption events (TDEs) occur when the gravitational field of a black hole (BH) overcomes the internal gravity of a star that approaches the BH's tidal radius, $R_{\rm T}$. Early theoretical studies (e.g. Frank & Rees 1976; Evans & Kochanek 1989) suggested that ∼50 per cent of the stellar material is unbound and ejects into the interstellar medium, but the remaining material settles into an accretion disc to be consumed by the BH. Spectral profile, intensity, and duration of emission from the accretion disc vary greatly depending upon the impact parameters of the encounter, the disrupted star structure, mass, and BH mass (e.g. Guillochon & Ramirez-Ruiz 2013; Malyali, Rau & Nandra 2019). While the rate of discovery of TDEs has increased at all wavelengths since the first candidate observation in X-rays (Bade, Komossa & Dahlem 1996), ultraviolet (Gezari et al. 2006), γ-rays (Bloom et al. 2011), and optical (van Velzen et al. 2011), optical observations have dominated recent discoveries (e.g. Gezari 2021). The increase in optical detections in the last decade is due to the introduction of high-cadence optical surveys, regularly revisiting wide areas of sky. Optical facilities involved in TDE detection include Sloan Digital Sky Survey (SDSS; Frieman et al. 2008), Panoramic Survey Telescope and Rapid Response System (PanSTARRS, Chambers et al. 2016), Palomar Transient Factory / intermediate (PTF/iPTF, Law et al. 2009; Masci et al. 2017), All Sky Automated Survey for SuperNovae (ASAS-SN, Kochanek et al. 2017), Optical Gravitational Lensing Experiment (OGLE, Udalski, Szymański & Szymański 2015), Asteroid Terrestrial-impact Last Alert System (ATLAS, Tonry et al. 2018), *Gaia* (Gaia Collaboration 2016), and Zwicky Transient Facility (ZTF; Bellm et al. 2019b). Even so, TDEs remain rare, but the depth and duration of archive data now permit limits to be placed on TDE rates.

Intermediate-mass black holes (IMBHs) are compact objects, with masses between those of stellar mass and supermassive black holes (SMBHs), i.e. $\sim 100\,M_\odot < M_{\rm BH} < 10^6\,M_\odot$. IMBHs are theorized to form in a number of ways (see Greene, Strader & Ho 2020), but their formation through mergers in dense stellar clusters (e.g. Miller & Hamilton 2002; Portegies Zwart & McMillan 2002) is key to why compact stellar systems (CSSs) have, to date, been focused on as potential hosts. Merging of BHs in dense stellar environments (e.g. Rodriguez et al. 2018, 2019; Di Carlo et al. 2021; González et al. 2021) has gained renewed interest since the first detection of a gravitational wave event leading to a remnant of IMBH mass (Abbott et al. 2020).

The authors also note a recent paper by Gomez & Gezari (2023), who carried out a search for white dwarf (WD)-based TDEs, suspected to be associated with IMBHs and have similar signatures to Type 1a supernova (SN). These authors did not detect any conclusive events in the ZTF data, based on their specific selection criteria. Similarly, Tang et al. (2024) searched for TDEs in a sample of nearly 4000 GCs in the Next Generation Virgo Cluster Survey (NGVCS), but did not detect any potential TDEs in their sample.

Within this work, we consider two types of CSSs exhibiting high stellar density, which are potentially hosts to IMBHs

★ E-mail: mnorris2@uclan.ac.uk

or SMBHs: globular clusters (GCs) that dominate our sample by number and ultracompact dwarfs (UCDs). The characteristics of UCDs place them between GCs and and compact ellipticals (cEs) in the mass/size parameter space (see e.g. Norris et al. 2014).

GCs generally form at high z, exist almost exclusively in galaxy haloes, and have masses $\lesssim 10^6$ M$_\odot$, with effective radii $R_e \lesssim 10$ pc.

UCDs have masses $\sim 10^6$–10^8 M$_\odot$ and size 10 pc $\lesssim R_e \lesssim$ 100 pc. Current research (e.g. Norris et al. 2015; Pfeffer et al. 2016) suggests multiple formation paths where UCDs represent a continuation of the high-mass end of GCs, or the tidally stripped remnant of a nucleated dwarf galaxy (Bekki, Couch & Drinkwater 2001). Most studies suggest a composite UCD population of the two formation methods (e.g. Norris & Kannappan 2011; Norris et al. 2014; Pfeffer et al. 2016), with both present below a star cluster formation limit of $M_\star \lesssim 5 \times 10^7$ M$_\odot$ (Norris et al. 2019). SMBHs have been detected in five (putative stripped nucleus type) UCDs (Seth et al. 2014; Ahn et al. 2017, 2018; Afanasiev et al. 2018) with upper limits in two UCDs determined by Voggel et al. (2018). More recently, Pechetti et al. (2022) suggest the presence of an IMBH $\sim 10^5$ M$_\odot$ in a stripped nucleus UCD around M31. Our search is thus well placed to detect both IMBHs and SMBHs in UCDs formed as stripped remnants.

The observational data for this analysis were obtained from the ZTF (Bellm et al. 2019a) based around the Palomar 48-inch Schmidt telescope (Samuel Oschin telescope). The ZTF is ideally suited to the detection of optical transients from unclassified sources. This is due to the cadence of its public survey observations, where the project aims to complete repeat visits of the entire Northern hemisphere every three nights. This allows detection of transients of the order of days, while the dual-band observations (g and r) allow colour information to be obtained. To the date of this paper, the ZTF had been credited with the initial discovery of more optical TDE signatures than any other single facility, i.e. 46 of 77 transients classified as TDEs in the Transient Name Server (TNS). There is also a good synergy of ZTF with the deeper PanSTARRS data, in terms of checking any off-nuclear TDEs observed for the presence of colocated CSS.

This project aims to add to the area of research that explores potential formation paths of both CSSs and IMBHs, by searching for TDE signatures of IMBHs within the CSS outlined. Detection of new candidate IMBHs, or provision of supplementary evidence for the presence of existing candidates, in CSS environments will assist in constraining hypotheses not only of CSS formation, but also of BH formation in dense cluster environments, as detailed above.

This document is structured to outline first the sample data used, including both the host galaxy selection and associated cone search definition (Section 2), followed by details of the light-curve extraction from the ZTF archives, through the ALeRCE broker, including filtering and categorization details (Section 3). An analysis of the implications of our findings is outlined in the discussion (Section 4).

2 SAMPLE

Our starting sample was drawn from the HyperLeda data base (Makarov et al. 2014). The criteria for sample selection was defined by the need to follow up any off-nuclear TDEs observed using PanSTARRS data, and to ensure completeness of our host galaxy data.

The upper limit to GCs has been proposed to be around $M_v = -13$ (Norris & Kannappan 2011; Norris et al. 2019), and at an upper distance limit of 120 Mpc this equates to an apparent magnitude of $m_v = 22.4$ mag, giving a good probability of detection in PanSTARRS with a 5σ, g-band limit of 23.3 mag. The original LEDA data base (i.e. the precursor of the HyperLeda catalogue) was used as the basis for the Third Reference Catalogue of Bright Galaxies (de Vaucouleurs et al. 1991) that was defined as complete to 15.5 mag and has subsequently been augmented with additional mission data to provide the homogenized data set seen in the HyperLeda data base. At this completeness limit for the HyperLeda data base, with an upper distance limit of 120 Mpc, gives a distance modulus of 35.4, and an upper limit on the absolute B magnitude of the host galaxies of $M_B = -20$. Therefore, we expect the input galaxy sample to be close to complete to $M_B = -20$ within the survey volume. This limit therefore rejects the vast majority of galaxies; however, such low-mass galaxies have very sparsely populated high-mass GC populations (e.g. van den Bergh 2006) and would tend not to produce GCs of masses where large IMBHs would be expected (e.g. Lützgendorf et al. 2013).

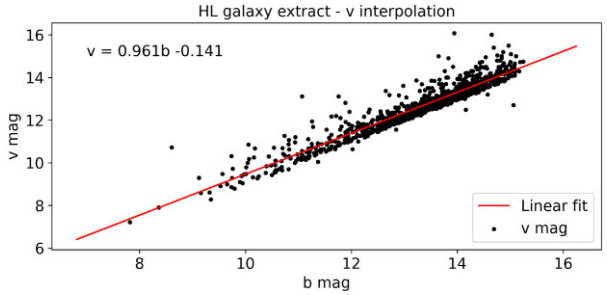

Figure 1. HyperLeda galaxy extract, apparent V mag versus B mag. ∼25 per cent of entries had existing measured values, so a simple linear interpolation from these was used to estimate missing V mag values.

The full criteria used for the sample of CSS host galaxies that could be cross-matched with alerts was as follows:

(i) *objtype* = 'G': ensure object is defined as a galaxy.
(ii) 26.5 < *modbest* < 35.4: best estimate of distance modulus. Gives distance 2 Mpc $\leq D \leq$ 120 Mpc. The lower limit takes the sample just outside of Andromeda (M31) to reduce clutter and filtering of oversize objects. The upper limit for host galaxies was set as discussed above.
(iii) *de*2000 > −30: limit on declination δ imposed by the use of the ZTF facility based in a northerly latitude.
(iv) Bmag < −20: Using the a threshold on absolute Bmag ensured rejection of smaller galaxies without significant CSS populations.

The initial sample returned included 4812 host galaxies ($A_g <$ 2.1 mag). However, to avoid regions of high galactic extinction, a limit of $A_g < 0.3$ mag was imposed, after which 3714 galaxies (∼77 per cent) remained.

As some of these galaxies lacked measured V-band magnitudes, a linear relationship between m_B and m_V, based on those galaxies with both, was estimated (see Fig. 1).

Using these values with the HyperLeda distance modulus, the absolute M_V was used to determine the specific frequency, S_N, of the GC/CSS population using the trend determined by Peng et al. (2008, table 3) from sample bins for their Virgo cluster (ACSVCS) galaxies. (see Fig. 2). Finally, using S_N, the relation detailed in Harris & van den Bergh (1981) between GC population and galaxy V-band luminosity was rearranged to estimate the number of GCs hosted by each galaxy in our sample, giving

$$N_{GC} = \frac{S_N}{10^{0.4(M_V+15)}} \quad (1)$$

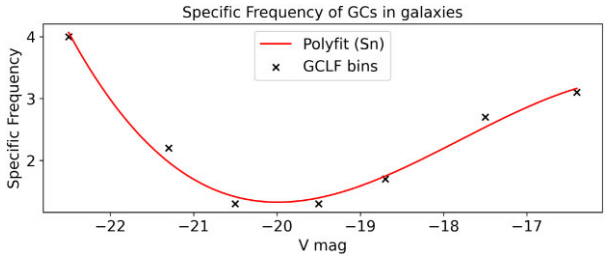

Figure 2. Specific frequency, S_N, defined by Harris & van den Bergh (1981), of GCs from bins measured by Peng et al. (2008). S_N is numbers of clusters per unit galaxy luminosity. A polynomial fit was made to estimate S_N for our galaxy sample.

and from this the total number of GCs hosted by the 3714 galaxies in the sample was estimated as

$$N_{\rm GC,Total} = \sum \frac{S_{\rm N}}{10^{0.4(M_V+15)}} \approx 2.8 \times 10^6. \quad (2)$$

We then estimated the number of GCs above a mass of 10^6 $M_\odot$ for each galaxy, following the process based on Jordán et al. (2007, figs 9 and 11, and equation 18). It is observed that the turnover magnitude of the approximately Gaussian globular cluster luminosity function (GCLF) is only weakly dependent on the host galaxy mass (Jordán et al. 2007). Hence, given the limited galaxy mass range sampled here we use a fixed value of $\mu_g = -7.2$ mag. In contrast, the dispersion of the GCLF is observed to vary sufficiently that we calculate an individual value for each galaxy following the relation $\sigma_g = 1.14 - [0.1 \times (M_{B,\rm gal} + 20)]$ from Jordán et al. (2007).

With these normal distribution parameters, for each host galaxy, we calculated the average number of GCs hosted which would be above a mass of 10^6 $M_\odot$. For this we used a g-band mass-to-light ratio of 3.25 from Maraston (1998, 2005), in respect of an old (10 Gyr), metal-poor ([Z/H] $= -1.35$) population based on a Salpeter IMF. We estimate the number of GCs above a mass of 10^6 $M_\odot$ as $N_{\rm gc,>1E6} \approx 2.4 \times 10^5$.

Consolidated light curves for transient alert objects were taken from the public alert archives from the period of the first phase of the ZTF programme (ZTF-1), lasting 30 months from March 2018 to September 2020, with additional data from October 2020 to November 2023. The ZTF facility aims to provide a full northern-sky survey cadence of 3 d; however, to account for inevitable gaps in observational coverage, the alert streams for potential GCs had a correction applied based on observations of the host galaxy.

A recent publication by Bandopadhyay et al. (2024) details simulations which suggest the time to peak for TDEs is determined 'almost exclusively' by the mass of the BH. They further suggest the time to peak is proportional to the square root of $M_{\rm BH}$, with full disruption of larger stars being the most luminous, but partial disruptions potentially lasting 'longer'. Their estimate for $M_{\rm BH} = 10^6$ $M_\odot$ is 30 d to peak and would give a peak time for $M_{\rm BH} = 10^5$ $M_\odot$ of 9 d, and $M_{\rm BH} = 10^4$ $M_\odot$ of 3 d. The fall-time of the curve is normally seen to follow roughly $-5/3$ power-law decay, but can be longer for partial disruptions (Mummery et al. 2024), so if we assume the fall-time is a few times the time to peak, we should observe $M_{\rm BH} > 10^4$ $M_\odot$, although $M_{\rm BH} < 10^4$ $M_\odot$ may be marginal, and difficult to classify. Based on this, a threshold of 9 d or more (i.e. 3 d × 3 d nominal cadence) was defined as a ZTF 'gap'. This was judged to be an extremely conservative estimate of the minimum amount of time a TDE around an IMBH should remain observable given the ZTF magnitude limit. The sum of gaps for each host target was deducted from the total observation period used in the final TDE rate estimation (see Section 4).

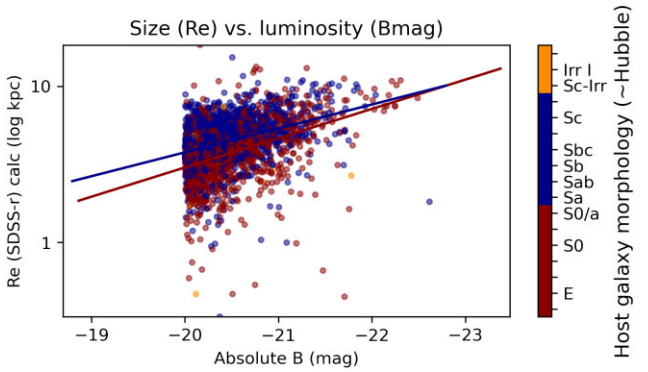

Figure 3. Size (R_e) versus B-mag plot used to estimate the effective radius of host galaxies, for which SDSS Petrosian R_{50} and R_{90} magnitudes were not available.

3 TRANSIENT ALERT ANALYSIS

Using the ZTF alert archive, we searched around the host galaxy positions to identify isolated alerts outside the galaxy nucleus, and also to check for misclassified TDEs in the search area. TDEs involving SMBH have been observed to peak at $-22 \lesssim M_V \lesssim -17$ (e.g. van Velzen et al. 2020; Hammerstein et al. 2023). This peak is attained over a period of ∼1 month, and the TDE remains visible for many months. At the outer limit of our survey volume (<120 Mpc) this gives a peak of ≃16 mag. Consequently, in the absence of internal dust, given the ZTF median sensitivity of 20.8 mag in g band, 20.6 mag in r band (Bellm et al. 2019b) we expect any SMBH TDEs in the search region to be observable. As noted by Metzger & Stone (2016), there is a weak dependence of peak luminosity on $M_{\rm BH}$, but adiabatic losses from radiation passing through the outer envelope of ejecta in lower mass BH interactions may suppress the peak optical luminosity. This is due to the model where post-peak TDE light curves follow the matter fallback rate onto the BH, although there is some debate over this $M_{\rm BH}$ correlation (e.g. Nicholl et al. 2020). Nevertheless, we assume a nominal 2–3 mag reduction in apparent magnitude compared to current SMBH observations, and given the cadence and magnitude limit of the ZTF, a minimum observability period of ∼9 d for IMBH related TDEs was not considered unreasonable (e.g. Angus et al. 2022).

SDSS parameters were downloaded for each of the host galaxies where available. Following the prescription determined by Graham et al. (2005), the effective radius R_e of the galaxy was determined in relation to the SDSS Petrosian magnitudes R_{50} and R_{90} through

$$R_e \approx \frac{R_{50}}{1 - P_3(R_{90}/R_{50})^{P_4}}, \quad (3)$$

where P3 and P4 equal 8.0×10^{-6} and 8.47, respectively. The SDSS coverage was 2602 entries of the 3714 original host galaxies in the list, and so a linear fit to the B-mag of the host was estimated from the available R_e values following a similar logic to that outlined by Shen et al. (2003), to calibrate the R_e versus B-mag relation (Fig. 3). A split on host galaxy morphology was included at type code = 0 (S0/a).

Although the extent of a GC system relative to its host galaxy varies between galaxy type and mass, many authors have observed and assumed values in the range 7–10R_e (e.g. Faifer et al. 2011; Forbes 2017; Bílek, Samurović & Renaud 2019) and thus a value of

Table 1. Summary of ZTF alert object classifications.

Count	Sub count	Description
2135		Post-filter galaxies with ZTF alert objects
6913		Distinct ZTF alert objects
4741		Objects with Gaia parallax
289		TNS classified entries
	161	TNS SN type II/pec/P/b/n/1b/1c
	122	TNS SN type 1a
	3	Other TNS (ILRT/gap/LRN)
	1	Nova
	2	Tidal disruption event (nuclear)
1900		TNS unclassified transients
	990	Spurious (minimal transients, no distinct curve)
	785	Nuclear proximity (bulge and nuclear transients)
	58	Spiral arm/halo location
	21	Background galaxy AGN
	14	Star/Galaxy artefacts
	13	Indeterminate (no curve)
	11	Star (variable)
	8	+ ve template (SN occurred in ZTF ref. image)

$10R_e$ was assumed here. This value was used to ensure coverage of all GCs associated with a host galaxy by estimating the galaxy extent and ultimately set the search cone radius for alerts.

The cone search was applied against the ALeRCE (Automatic Learning for Rapid Classification of Events) host site using API scripts (Förster et al. 2021). Alerts with ZTF real/bogus rating $rb < 0.5$ were rejected, and remaining alert data downloaded for further analysis. For all alerts within a galaxy region, ZTF metadata was used to aid transient candidate prioritizing. This included the number of alerts within a region, a count of unique ZTF transient objects associated with the alerts and the maximum detections associated with a single object. The latter was used to reject objects where the detection history was less than 3, i.e. a minimum of three transient alerts were required, and single detections were ignored. Alerts in proximity (<2 arcsec) of solar system objects were also rejected.

Final filtering was achieved by rejecting ZTF alert objects within 2 arcsec of *Gaia* DR3 objects with a measured parallax (4741), on the assumption these objects are 'local'. Additionally, ZTF objects previously classified in TNS (289) were only given a cursory inspection.

The volume around galaxy peripheries furnished alerts with various light curves, including a large number of supernova (SN) (see Table 1). The alert objects were explored by cross-matching with external databases, where additional data extracted included TNS information, and correlation with SIMBAD (Wenger et al. 2000) and GAIA databases.

The environment and light curves of all ZTF alert objects (1900) in host galaxies associated with the remaining alerts (65035) were inspected for evidence of TDEs. This was achieved using ZTF alert data in conjunction with ALeRCE ZTF Explorer (see https://alerce.online/). An example of ZTF alert data is shown in Fig. 4 for galaxy ESO540-025, a Type 1a SN. The figure shows visualization of ZTF alert history with 1′ final alert image cut-outs and PS combined gri_{PS1} image, all centered on the alert position..

The process followed to classify the transients associated with the ZTF alert objects, involved inspection of all of the 1900 non-*Gaia* parallax light curves. An initial pass of the light curves discounted those based on their proximity to the nucleus of the host galaxy (785). A second criteria applied at this time was to discount spurious transients (990), defined as objects which nominally showed no obvious signs of a curve, had minimal total (<4) real detections or contained multiple (>2) intermediate non-detections between real detections.

For the remaining 125 ZTF alert objects, further scrutiny was applied. Each of these were placed in bins with the following precedence:

(i) Artefact: These are clear imaging artefacts in either the science or template images, for example, even after masking caused by diffraction spikes from a nearby bright star.

(ii) Star: Stellar objects (some variable) picked up in field. Confirmed with Gaia proximity and source extraction assessment.

(iii) Background galaxy: Galaxies confirmed in background to host galaxy as viewed in PanSTARRS imagery and through source extraction assessment.

(iv) Positive template: Some ZTF objects were active supernova events while reference templates were being generated early in 2018. Subsequent science imagery consists of dimmer magnitude values, and hence constant negative difference alerts. These were scrutinized but ignored.

(v) Spiral/halo: Transients located predominantly in spiral arms, often star-forming regions or late-type galaxies or bulges of early-type galaxies, in addition to some halo transients showing no distinct curve. A minimal number (<10) of the objects in this category showed distinct light curves and were given further scrutiny, validating the rise/fall time (typically longer than SNe), colour ($-0.4 \lesssim g - r \lesssim 0$), and colour evolution (which for TDEs is practically constant) of the object (van Velzen et al. 2021), in addition to the location relative to the host galaxy. All were rejected.

(vi) Indeterminate: Remaining (miscellaneous) bin of light curves, defying classification under other criteria, but with no definitive shape to alerts associated with ZTF object, often with multiple intermediate non-detections.

Further details and examples of the above classifications are included in Appendix A.

No halo TDEs were evident in our search of alerts proximal to filtered galaxies out to 120 Mpc, although two TNS classified nuclear TDEs were noted (ZTF18aabkvpi and ZTF20aamaczu in NGC3800). At the date of this report, a search of the TNS data base also showed 77 transients classified as TDEs, the discovery of 46 of which were credited to ZTF data. The light curve from the closest TDE (AT2019qiz, ∼66 Mpc, Forster 2019; Nicholl et al. 2020; Hung et al. 2021) is an example associated with an SMBH (only 1 dex outside the IMBH mass range). There are many variables associated with both BH and disrupted star mass, and impact parameters of the encounter, leading to a range of outcomes and profile evolution for the emissions from the event (e.g. Ulmer 1999; Guillochon & Ramirez-Ruiz 2013; Malyali et al. 2019). Nevertheless, to a first order we can argue that TDEs present in the region searched would be detected within this data. However, as noted in Section 2, if the simulations of Bandopadhyay et al. (2024) are correct, then with our conservative observability limits (i.e. >9-d threshold defined as an gap in observations), detection of TDEs associated with IMBH$<10^4$ would be marginal.

4 DISCUSSION

Early predictions of TDE rates, albeit for SMBHs and solar mass stars, were quoted at $n_{TDE} \approx 10^{-4}\,gal^{-1}\,yr^{-1}$, e.g. Frank & Rees (1976); Ulmer (1999). Stone & Metzger (2016) note observational results suggest an order of magnitude lower rate at $n_{TDE} \approx$

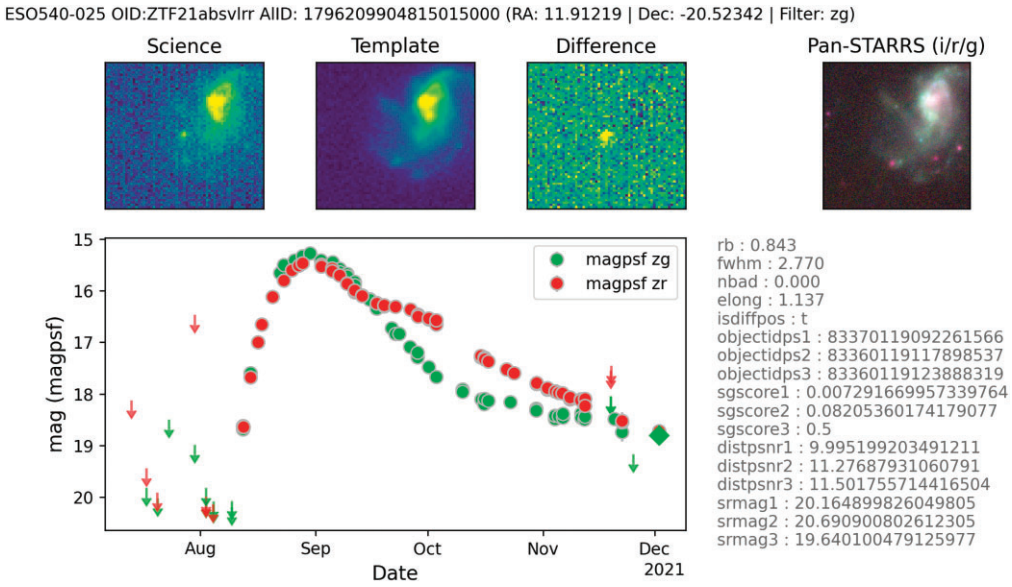

Figure 4. Visualization of ZTF alert data, shown for ZTF21absvlrr within ESO540-025. 1' cutouts for science, reference, and difference images are shown alongside PanSTARRS colour (*gri*) image. ID for latest alert ID (AlID) given and ZTF alert metadata included. This candidate was classified in the TNS records as a Type 1a SN.

10^{-5} gal^{-1} yr^{-1}. Recent observations using ZTF data have provided some validation to this lower rate, with an average optical rate of $\approx 3.2 \times 10^{-5}$ gal^{-1} yr^{-1} determined by Yao et al. (2023). Conversely, as the rate is sensitive to the central density profile of a galaxy, Wang & Merritt (2004) suggested for systems such as nucleated dwarfs, with steep nuclear density profiles, the rate may be higher than predicted by Frank & Rees (1976) at $n_{\rm TDE} \approx 10^{-3}$ gal^{-1} yr^{-1}. This latter case is particularly relevant for the composite population of CSSs; thus, we compare the above rates with an upper limit based on our non-detection of TDEs.

The period of data sampling, $t_{\rm ZTF}$, for the ZTF alert pipeline was taken to be mid-March 2018 to mid-November 2023 or 68 months (5.7 yr); however, as detailed in Section 2, sample periods of GC population observations were adjusted for host galaxy observability. Using these adjusted time-scales, and non-detection of TDEs in the total notional clusters of $N_{\rm GC,Total} \approx 2.8 \times 10^6$, we estimate a total TDE upper limit of

$$N_{\rm TDE,Total} < \frac{1}{N_{\rm GC,Total} \times t_{\rm ZTF}} \lessapprox 2 \times 10^{-7}\,{\rm CSS}^{-1}\,{\rm yr}^{-1}, \quad (4)$$

which is ∼2 dex below the lowest literature detection limit for galaxies. This implies either ∼100 TDEs in this sample occurred but were undetected, or the TDE rate in CSSs is considerably lower than in galaxies.

Despite attempting to ensure object visibility, it is possible non-detections may occur if the immediate vicinity of the BH is optically thick (i.e. Panagiotou et al. 2023). However, a surplus of gas and dust is at odds with the view of GCs, as excess material is considered to be used or ejected from these systems during their primary star formation episode. Conversely, for CSS formed through tidal stripping, more gas and dust may temporarily be present in the core due to inflows after interaction of the progenitor with a larger galaxy (e.g. Janz et al. 2016; Du et al. 2019), although in general, dust is not expected to be significant. No significant amount has been conclusively detected in any objects of GC/UCD mass. It does not survive in GCs/UCDs, being pushed out by radiation pressure rapidly (e.g. time-scales of $\sim 10^5$ yr; McDonald 2009), the same is true of a stripped CSS once it has lost its dark matter halo and the potential becomes that provided by the stars alone. It is possible that a thick disc would be sufficient to absorb optical emissions, although statistically, face on viewing should have given rise to detections (see Dai et al. 2018).

In the case where the TDE rate is lower in CSSs than galaxies, there are two possible explanations; IMBH do not exist in CSS, or IMBH do exist, but the TDE rate is suppressed in this environment by some unknown mechanism.

When considering whether IMBH exist in CSS, it is useful to split the composite population into massive clusters and tidally stripped galaxies. It has long been thought GCs (and thus massive clusters) may harbour nuclear BH and at the lower end of the CSS mass scale this view has tantalizing implications. If central BHs form in clusters following a similar process to larger galaxies, we can extrapolate BH mass-scaling relationships to intermediate scales. There is, however, a lack of conclusive evidence of nuclear BH in clusters. Early studies suggested formation of IMBH in clusters was possible through core collapse and runaway mergers of massive stars (Portegies Zwart & McMillan 2002), or repeated merging of mass-segregated BHs (Miller & Hamilton 2002). Nevertheless, numerical simulations (e.g. Giesler, Clausen & Ott 2018) show dynamical interactions in cluster cores would eject many BHs before larger mass BH could 'grow' through mergers. X-ray emissions also seem prevalent in GCs (e.g. Strader et al. 2012), most associated with compact object related low-mass X-ray binaries (LMXB). Thus, an excess of dynamical mass compared to luminous mass, might be explained by a population of core segregated stellar mass BH and neutron stars rather than a single nuclear IMBH. Several examples exist of observational evidence fitting both scenarios (e.g. Vitral & Mamon 2021).

There is much evidence to suggest that the TDE rate in galaxies appears to be dominated by galaxies with a high surface mass density. Authors such as Graur et al. (2018, table 3) find TDE host properties $\approx 10^9$ M$_\odot$ kpc$^{-2} \leq \Sigma_{M_\star} \leq 10^{10}$ M$_\odot$ kpc^{-2}. Law-Smith et al. (2017) discuss the stellar mass density in relation to the Sérsic index as a broad indicator of the galaxy's light profile, and details in French

et al. (2020) suggest a range of $10^{10.5}$–10^{11} $M_\odot$ kpc^{-2}, although their findings are based on a detailed *Hubble Space Telescope* analysis of only four TDE hosts.

In comparison, we also find there is much evidence that the high-mass end of GCs/UCDs, i.e. those above a mass of 10^6 $M_\odot$, have surface mass densities comparable to galaxies, especially those formed through tidal stripping processes. For example, Norris et al. (2014, fig. 14) find for GCs/UCDs $> 10^6$ $M_\odot$ the surface mass density within $R_e \approx 10^9$ $M_\odot$ kpc^{-2} $\leq \Sigma_{M_\star} \leq 10^{11}$ $M_\odot$ kpc^{-2}. Additionally, in UCDs where detailed observations and analysis have suggested the presence of a black hole, noted in Section 1, the stellar density in the immediate proximity of the BH is shown to be high. For example, Afanasiev et al. (2018) find that Fornax-UCD3 has a stellar mass density of $\approx 2.5 \times 10^{10}$ $M_\odot$ kpc^{-2} within a pc of the centre. Ahn et al. (2018) find an order of magnitude greater surface mass density for M59-UCD3, and similarly for VUCD3 (Ahn et al. 2018).These comparisons support the assumption that the TDE rate in GCs/UCDs $>10^6$ $M_\odot$ will be comparable to the 'normal' rate in high surface mass density galaxies.

At the upper end of the CSS mass scale, considering UCDs or cEs formed through tidal stripping or cEs formed as low-mass galaxies, larger mass BHs are anticipated, and have been detected, as mentioned in Section 1. Bulges and cores surviving tidal threshing would have a nuclear BH mass related to the progenitor, and thus higher than expected for the remnant cluster mass. This is a differentiator of formation in the composite CSS population, and an example of core phenomenological parameters that are considered to remain unaffected by tidal stripping. Therefore, given the expected BH masses and high surface mass density, there is no reason to expect fewer TDEs in this type of environment than the galactic cores for which the theoretical rate has been measured. Authors such as Janz et al. (2015) have identified UCDs with increased dynamical to stellar mass ratios with nuclear SMBH, and if these have the same TDE rate as 'normal' galaxies, our non-detection allows us to set a limit on the number of stripped UCDs in the area searched.

In Section 2, we used the GCLF to estimate the number of GCs in the volume searched above a mass of 10^6 $M_\odot$, to be $N_{gc,>1E6} \approx 2.4 \times 10^5$. Further to this, we then use an average optical TDE rate of $\approx 3.2 \times 10^{-5}$ gal^{-1} yr^{-1} determined by Yao et al. (2023), and also assume a conservative 40 per cent ZTF observability figure over the 5.7 yr for the brighter and longer period TDEs involving SMBH in stripped UCDs. From this, we set an upper limit on the number of stripped UCDs populating the galaxies in the area searched as

$$N_{\rm GC,\,Strip} \lessapprox \frac{1}{3.2 \times 10^{-5} \times 5.7 \times 0.4} \lessapprox 1.4 \times 10^4. \quad (5)$$

We estimate that this represents an upper limit for the fraction of UCDs, as a proportion of the population of GCs over 10^6 $M_\odot$, to be

$$\varphi_{\rm GC,strip} \lessapprox 1.4 \times 10^4 / 2.4 \times 10^5 \lessapprox 5.8 \ \text{per cent}. \quad (6)$$

This is in reasonable agreement with the semi-analytical model and observations of Pfeffer et al. (2016), who suggested stripped nucleus UCDs account for 2.5 per cent of the GC/UCD total between 10^6 and 10^7 $M_\odot$ increasing to 40 per cent above 10^7 $M_\odot$.

The approach utilized here of searching for TDEs in CSS will naturally lead to detections or increasingly stringent upper limits as the duration of ZTF observations increases. In addition, the advent of the Vera Rubin Observatory (Legacy Survey of Space and Time, LSST) will dramatically increase the survey volume probed thanks to its greater depth (∼24 mag) (Ivezić et al. 2019) and approximately halved seeing (0.75 versus 1.4).

5 CONCLUSIONS

In this paper, we have searched for optical transients consistent with being TDEs associated with IMBHs/SMBHs in CSSs using 68 months of ZTF archive data. The search area consisted of the region within $10R_e$ of massive galaxies ($M_B < -20$ mag) at distance 2 Mpc $\leq D \leq$ 120 Mpc, notionally to encompass the entire population CSSs hosted by the galaxies. No transient alert profiles were found to be consistent with being non-nuclear TDEs and hence we conclude an upper limit for the rate of TDEs in CSS is $n_{\rm TDE,Total} \lessapprox 10^{-7}$ CSS^{-1} yr^{-1}. We note that this rate is 2 dex below the observed TDE rate involving SMBH interacting with solar mass main-sequence stars in the nucleus of galaxies. We also estimated an upper limit on the number of UCDs formed through tidal stripping processes to be $N_{\rm GC,Strip} < 1.4 \times 10^4$, which we determined represents an upper limit for the fraction of tidally stripped type UCDs as a proportion of the population of CSSs over 10^6 $M_\odot$ as $\varphi_{\rm GC,strip} < 5.8$ per cent.

ACKNOWLEDGEMENTS

We thank the anonymous referee for their helpful and insightful comments.

This work is based on observations obtained with the Samuel Oschin 48-inch Telescope at the Palomar Observatory as part of the Zwicky Transient Facility project. ZTF is supported by the National Science Foundation under grant no. AST-1440341 and a collaboration including Caltech, IPAC, the Weizmann Institute for Science, the Oskar Klein Center at Stockholm University, the University of Maryland, the University of Washington, Deutsches Elektronen-Synchrotron and Humboldt University, Los Alamos National Laboratories, the TANGO Consortium of Taiwan, the University of Wisconsin at Milwaukee, and Lawrence Berkeley National Laboratories. Operations are conducted by COO, IPAC, and UW.

We acknowledge the usage of the HyperLeda data base (http://leda.univ-lyon1.fr/; Makarov et al. 2014).

We acknowledge the use of data from the ALeRCE project (https://alerce.science).

We acknowledge the use of data from the Sloan Digital Sky Survey (SDSS; http://www.sdss.org/). Funding for the SDSS has been provided by the Alfred P. Sloan Foundation, the Participating Institutions, the National Aeronautics and Space Administration, the National Science Foundation, the U.S. Department of Energy, the Japanese Monbukagakusho, and the Max Planck Society.

DATA AVAILABILITY

The data used in this analysis are available at https://github.com/Pommers/IMBH.

REFERENCES

Abbott R. et al., 2020, Phys. Rev. Lett., 125, 101102
Afanasiev A. V. et al., 2018, MNRAS, 477, 4856
Ahn C. P. et al., 2017, ApJ, 839, 72
Ahn C. P. et al., 2018, ApJ, 858, 102
Angus C. R. et al., 2022, Nat. Astron., 6, 1452
Bade N., Komossa S., Dahlem M., 1996, A&A, 309, L35
Bandopadhyay A. et al., 2024, ApJ, 961, L2
Bekki K., Couch W. J., Drinkwater M. J., 2001, ApJ, 552, L105
Bellm E. C. et al., 2019a, PASP, 131, 018002
Bellm E. C. et al., 2019b, PASP, 131, 068003

Bílek M., Samurović S., Renaud F., 2019, A&A, 625, A32
Bloom J. S. et al., 2011, Science, 333, 203
Chambers K. C. et al., 2016, PanSTARRS survey, preprint (arXiv:1612.05560)
Dai L., McKinney J. C., Roth N., Ramirez-Ruiz E., Miller M. C., 2018, ApJ, 859, L20
de Vaucouleurs G., de Vaucouleurs A., Corwin H. G., Jr, Buta R. J., Paturel G., Fouque P., 1991, Third Reference Catalogue of Bright Galaxies. Springer, New York, NY
Di Carlo U. N. et al., 2021, MNRAS, 507, 5132
Du M. et al., 2019, ApJ, 875, 58
Evans C. R., Kochanek C. S., 1989, ApJ, 346, L13
Faifer F. R. et al., 2011, MNRAS, 416, 155
Forbes D. A., 2017, MNRAS, 472, L104
Forster F., 2019, Transient Name Server Discovery Report, 2019-1857, 1
Förster F. et al., 2021, AJ, 161, 242
Frank J., Rees M. J., 1976, MNRAS, 176, 633
French K. D., Arcavi I., Zabludoff A. I., Stone N., Hiramatsu D., van Velzen S., McCully C., Jiang N., 2020, ApJ, 891, 93
Frieman J. A. et al., 2008, AJ, 135, 338
Gaia Collaboration, 2016, A&A, 595, A1
Gezari S., 2021, ARA&A, 59
Gezari S. et al., 2006, ApJ, 653, L25
Giesler M., Clausen D., Ott C. D., 2018, MNRAS, 477, 1853
Gomez S., Gezari S., 2023, ApJ, 955, 46
González E., Kremer K., Chatterjee S., Fragione G., Rodriguez C. L., Weatherford N. C., Ye C. S., Rasio F. A., 2021, ApJ, 908, L29
Graham A. W., Driver S. P., Petrosian V., Conselice C. J., Bershady M. A., Crawford S. M., Goto T., 2005, AJ, 130, 1535
Graur O., French K. D., Zahid H. J., Guillochon J., Mandel K. S., Auchettl K., Zabludoff A. I., 2018, ApJ, 853, 39
Greene J. E., Strader J., Ho L. C., 2020, ARA&A, 58, 257
Guillochon J., Ramirez-Ruiz E., 2013, ApJ, 767, 25
Hammerstein E. et al., 2023, ApJ, 942, 9
Harris W. E., van den Bergh S., 1981, AJ, 86, 1627
Hung T. et al., 2021, ApJ, 917, 9
Ivezić Ž. et al., 2019, ApJ, 873, 111
Janz J., Forbes D. A., Norris M. A., Strader J., Penny S. J., Fagioli M., Romanowsky A. J., 2015, MNRAS, 449, 1716
Janz J. et al., 2016, MNRAS, 456, 617
Jordán A. et al., 2007, ApJS, 171, 101
Kochanek C. S. et al., 2017, PASP, 129, 104502
Law-Smith J., Ramirez-Ruiz E., Ellison S. L., Foley R. J., 2017, ApJ, 850, 22
Law N. M. et al., 2009, PASP, 121, 1395
Lützgendorf N. et al., 2013, A&A, 555, A26
Makarov D., Prugniel P., Terekhova N., Courtois H., Vauglin I., 2014, A&A, 570, A13
Malyali A., Rau A., Nandra K., 2019, MNRAS, 489, 5413
Maraston C., 1998, MNRAS, 300, 872
Maraston C., 2005, MNRAS, 362, 799
Masci F. J. et al., 2017, PASP, 129, 014002
McDonald I., 2009, PhD thesis, Keele University, UK
Metzger B. D., Stone N. C., 2016, MNRAS, 461, 948
Miller M. C., Hamilton D. P., 2002, MNRAS, 330, 232
Mummery A., van Velzen S., Nathan E., Ingram A., Hammerstein E., Fraser-Taliente L., Balbus S., 2024, MNRAS, 527, 2452
Nicholl M. et al., 2020, MNRAS, 499, 482
Norris M. A., Kannappan S. J., 2011, MNRAS, 414, 739
Norris M. A. et al., 2014, MNRAS, 443, 1151
Norris M. A., Escudero C. G., Faifer F. R., Kannappan S. J., Forte J. C., van den Bosch R. C. E., 2015, MNRAS, 451, 3615
Norris M. A., van de Ven G., Kannappan S. J., Schinnerer E., Leaman R., 2019, MNRAS, 488, 5400
Panagiotou C. et al., 2023, ApJ, 948, L5
Pechetti R. et al., 2022, ApJ, 924, 48
Peng E. W. et al., 2008, ApJ, 681, 197
Pfeffer J., Hilker M., Baumgardt H., Griffen B. F., 2016, MNRAS, 458, 2492
Portegies Zwart S. F., McMillan S. L. W., 2002, ApJ, 576, 899
Rodriguez C. L., Amaro-Seoane P., Chatterjee S., Rasio F. A., 2018, Phys. Rev. Lett., 120, 151101
Rodriguez C. L., Zevin M., Amaro-Seoane P., Chatterjee S., Kremer K., Rasio F. A., Ye C. S., 2019, Phys. Rev. D, 100, 043027
Seth A. C. et al., 2014, Nature, 513, 398
Shen S., Mo H. J., White S. D. M., Blanton M. R., Kauffmann G., Voges W., Brinkmann J., Csabai I., 2003, MNRAS, 343, 978
Stone N. C., Metzger B. D., 2016, MNRAS, 455, 859
Strader J., Chomiuk L., Maccarone T. J., Miller-Jones J. C. A., Seth A. C., 2012, Nature, 490, 71
Tang V. L., Madau P., Bortolas E., Peng E. W., Feng Y., Guhathakurta P., 2024, ApJ, 963, 146
Tonry J. L. et al., 2018, PASP, 130, 064505
Udalski A., Szymański M. K., Szymański G., 2015, Acta Astron., 65, 1
Ulmer A., 1999, ApJ, 514, 180
van den Bergh S., 2006, AJ, 131, 304
van Velzen S. et al., 2011, ApJ, 741, 73
van Velzen S., Holoien T. W. S., Onori F., Hung T., Arcavi I., 2020, Space Sci. Rev., 216, 124
van Velzen S. et al., 2021, ApJ, 908, 4
Vitral E., Mamon G. A., 2021, A&A, 646, A63
Voggel K. T. et al., 2018, ApJ, 858, 20
Wang J., Merritt D., 2004, ApJ, 600, 149
Wenger M. et al., 2000, A&AS, 143, 9
Yao Y. et al., 2023, preprint (arXiv:2303.06523)

APPENDIX A: LIGHT-CURVE CATEGORIZATION

As noted in the main text, visual classification of 1900 ZTF alert object light curves was carried out after initial filtering of the alerts. The categories were defined to facilitate an iterative process of object reduction, so that further scrutiny could be prioritized against objects of interest. As shown in the unclassified transients section of Table 1, these categories were defined as spurious, nuclear, spiral arm/halo located, background galaxy, imaging artefacts, stellar object, and positive template. The final category was indeterminate, for objects which defied classification in any of the previous bins. Examples of each of these categories are shown in Fig. A1.

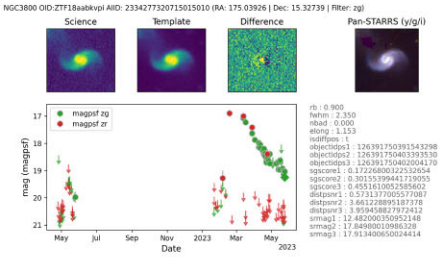

(a) One of the 2 TDEs observed in the sample. Both were nuclear TDEs (non-halo) - included for reference purposes.

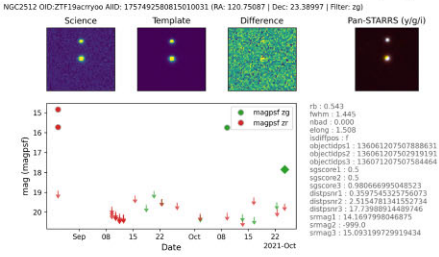

(b) Typical spurious alert. Minimal uncorrelated detections with multiple non-detections.

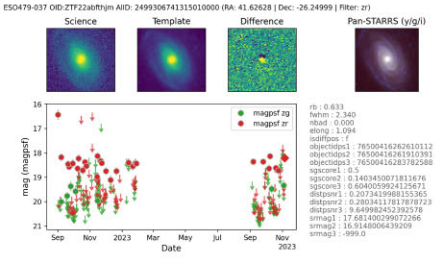

(c) Alerts in proximity to host galaxy nucleus.

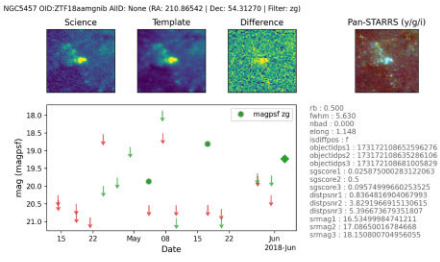

(d) Typical spiral arm 'clutter' causing spurious alerts.

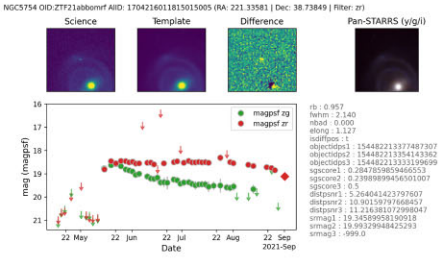

(e) Halo detection. As noted in the text, similar objects were given more scrutiny. This object rejected as unclassified SNe-type II, based on rise time and colour evolution.

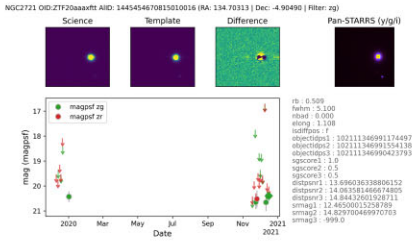

(f) Imaging artefact associated with stellar object.

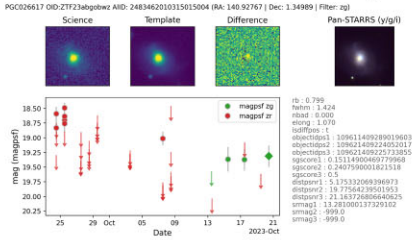

(g) Indeterminate alerting detections. No distinct curve, multiple intermediate non-detections.

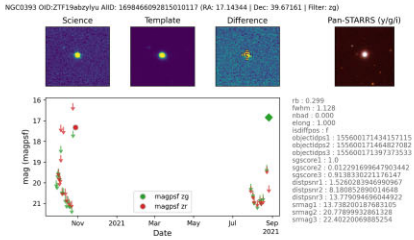

(h) Objects associated with 'local' variable star or stellar variation.

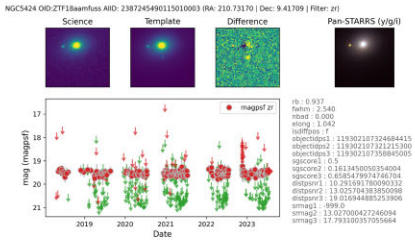

(i) Multiple alerts showing negative difference based on legacy positive template (i.e. transient during reference image generation).

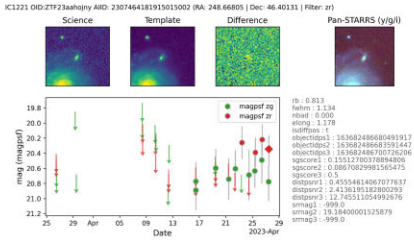

(j) Background galaxy or AGN associated alerts.

Figure A1. Example light curves, illustrating different categories (as detailed in main text) used during the ZTF alert object classification process.

This paper has been typeset from a TEX/LATEX file prepared by the author.